Stimulus-Evoked Intrinsic Optical Signals in the Retina: Spatial and Temporal Characteristics

Jesse Schallek,[1] *Hongbin Li,*[1] *Randy Kardon,*[2] *Young Kwon,*[2] *Michael Abramoff,*[2] *Peter Soliz,*[3] *and Daniel Ts'o*[1]

Purpose. To characterize the properties of stimulus-evoked retinal intrinsic signals and determine the underlying origins.

Methods. Seven adult cats were anesthetized and paralyzed to maximize imaging stability. The retina was stimulated with a liquid crystal display (LCD) integrated into a modified fundus camera (Topcon, Tokyo, Japan). The LCD presented patterned visual stimuli while the retina was illuminated with near infrared (NIR) light. The peristimulus changes in the NIR reflectance of the retina were recorded with a digital camera.

Results. Two stimulus-evoked reflectance signals in the NIR were observed: a positive signal, corresponding to a relative increase in reflectance, and a negative signal, corresponding to a relative decrease in reflectance. When presented with a positive-contrast stimulus, the negative reflectance signals showed a tight spatial coupling with the stimulated region of retina, whereas the positive signals arose in an adjacent region of the retina. Signals remained spatially confined to the stimulated region even when stimuli of much longer duration were used. In addition, the positive and negative signal polarities reversed when the stimulus contrast was inverted. Both signals showed a rise time on the order of seconds, similar to those observed in the mammalian neocortex. The spectral dependency of the signals on illumination was similar to the absorbance spectra of hemoglobin and the oximetric relationship.

Conclusions. The findings characterize the basic properties of stimulus-evoked intrinsic signals of the retina. These signals were generally similar to the more extensively studied cortical signals. Collectively, the data suggest a hemodynamic component to the intrinsic optical signals of the retina. (*Invest Ophthalmol Vis Sci.* 2009;50:4865–4872) DOI:10.1167/iovs.08-3290

Intrinsic signal optical imaging in the mammalian neocortex has been extensively used by brain researchers since its accelerated development in the 1980s.[1–3] The implementation of this technique has enabled researchers to examine the highly ordered organization of cortical maps. Intrinsic signal imaging measures optical reflectance changes associated with the activity of neural tissue. In the cortex, changes in reflectance are attributed to physiological changes in cerebral blood flow,[2,4] light-scattering,[5] and the oximetric signal.[1,2]

Similarly, studies in the retina have reported the presence of "fast intrinsic signals" that originate from the light-scattering properties of photoreceptors,[6] as well as optical changes from water and ion movements of active neurons.[5,7] Spectral reflectance changes also arise from the hemodynamics of blood flow[8] and the oximetric relationship.[9] Recently, several groups have identified the presence of slow, stimulus-evoked reflectance changes in the retina in vivo (Ts'o DY, et al. *IOVS* 2003;44:ARVO E-Abstract 2709; Ts'o DY, et al. *IOVS* 2004;45:ARVO E-Abstract 3495; Ts'o DY, et al. *IOVS* 2005;46:ARVO E-Abstract 2258; Ts'o DY, et al. *IOVS* 2006;47:ARVO E-Abstract 5899; Ts'o DY, et al. *IOVS* 2007;48:ARVO E-Abstract 1957; Ts'o DY, et al. *IOVS* 2008;49:ARVO E-Abstract 2006).[10–14] The reflectance signals are generated by intrinsic mechanisms, meaning injectable dyes are not needed to observe the functional regions. Although several groups have demonstrated the presence of intrinsic retinal signals, the biophysical origins of these signals are still uncertain.

We present data that describe the fundamental spatial and temporal characteristics of the signals. Our findings show that intrinsic optical signals in the near infrared (NIR), exist in the cat retina with robust signal strength nearly two orders of magnitude greater than seen in the cortex. Moreover, these signals demonstrate strong focal activations corresponding to regions of visually stimulated retina. We focused our efforts on characterizing the stimulus-dependent signals, to better elucidate their origins.[15]

Methods

Animals and Preparation

We investigated the retinas of seven adult healthy cats between the ages of 5 months and 5.5 years. The cats were initially anesthetized with ketamine HCl (10 mg/kg IM) followed by sodium thiopental (20 mg/kg IV, supplemented by a constant infusion of 1 to 2 mg/kg/h). The animals were then intubated with an endotracheal tube, paralyzed with vecuronium bromide (0.1 mg/kg/h), and artificially ventilated with room air. The electrocardiogram (ECG), electroencephalogram (EEG), temperature and expired CO_2 were monitored throughout the duration of the experiment. Neosynephrine (10%) and atropine (1%) were applied topically to dilate the pupil and inhibit accommodation. The corneas were fitted with low-power, 34.0-D lenses for protection against drying. Total corrective power was achieved with the internal optics of the fundus camera to optimize imaging of the retinal surface. Animals were secured in a stereotaxic frame for optical alignment with the fundus camera and to ensure the stability and consistency of imaging.

The following investigation on cats adhered to the ARVO Statement for the Use of Animals in Ophthalmic and Vision Research. Animals have been cared for in accordance with the Animal Welfare Act and the DHHS "Guide for the Care and Use of Laboratory Animals."

From the [1]Department of Neurosurgery, SUNY Upstate Medical University, Syracuse, New York; the [2]Department of Ophthalmology and Visual Science, University of Iowa, Iowa City, Iowa; and [3]VisionQuest Biomedical, Albuquerque, New Mexico.

Supported by National Institutes of Health NIBIB (National Institute of Biomedical Imaging and Bioengineering) Grant EB002843 and the Glaucoma Research Foundation.

Submitted for publication December 9, 2008; revised February 24, 2009; accepted July 15, 2009.

Disclosure: **J. Schallek**, None; **H. Li**, None; **R. Kardon**, P; **Y. Kwon**, P; **M. Abramoff**, None; **P. Soliz**, VisionQuest Biomedical (E); **D. Ts'o**, P

The publication costs of this article were defrayed in part by page charge payment. This article must therefore be marked "*advertisement*" in accordance with 18 U.S.C. §1734 solely to indicate this fact.

Corresponding author: Daniel Ts'o, Department of Neurosurgery, SUNY Upstate Medical University, 750 E. Adams Street, Syracuse NY 13210; tsod@upstate.edu.

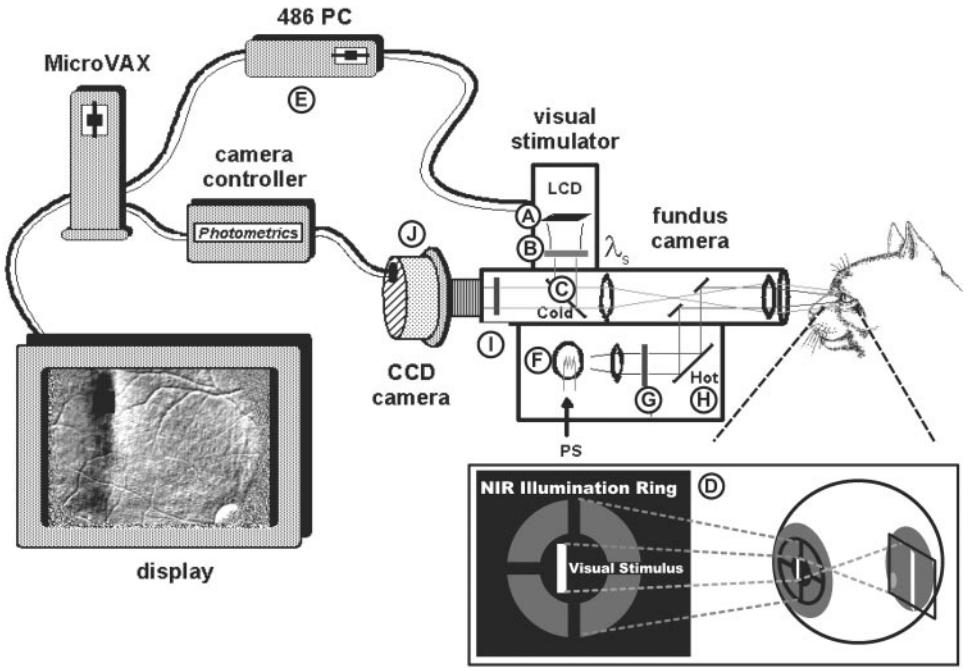

FIGURE 1. Schematic of the intrinsic signal imaging instrumentation. (A) Visual stimuli are generated on an LCD display. (B) The stimulus is filtered by a 540-nm wide-band filter. (C) The visual stimulus is merged into the optical pathway of the fundus camera by a cold mirror that reflects visible light at 45°. (D) The emitted aerial image shows the separation of the stimulus (center) and illumination (annulus) surround. (E) Stimulus patterns are generated by a computer running a graphics card (Number Nine, Cambridge, MA). (F) The illumination for the retina is provided by a tungsten incandescent bulb. (G) Illumination wavelengths are filtered by a bank of user-selectable NIR filters. (H) The illumination wavelengths are reflected by a hot mirror reflecting NIR wavelengths through an annular aperture. (I) Reflectance signals returning from the retina are also filtered by a long-pass filter that rejects visible light (stimulus energy). (J) NIR reflectance signals are collected by a cooled CCD camera, which sends data to a host computer for data storage.

Stimuli

The retina was optically stimulated through a modified fundus camera (Topcon, Tokyo, Japan; Fig. 1). A small LCD (SONY) presented the visual stimulus generated by a custom program. The stimulus was filtered in series with an infrared blocking filter and a 540 ± 30-nm filter (540-nm center wavelength, 60-nm band-width at full-width, half-height [FWHH]; Edmund Optics, Inc., Barrington, NJ) then reflected from a dichroic mirror, through the original optical path of the fundus camera, into the subject's eye (Fig. 1). The stimulus set comprised bars oriented horizontally or vertically at different positions across the retina (Fig. 2). Unless otherwise noted, the patterned stimulus intensity was between 3 and 7.7 cd/m^2, and the background LCD level was 0.12 cd/m^2. The animals were adapted to the low-mesopic background level for an hour or more before imaging started. The stimulus background contrast was maximized to achieve a Michelson contrast of 96.8%. The stimulus was presented in four blocks of 4 to 18 randomized stimulus conditions per imaging session. Stimulus contrast, mean luminance, flicker frequency, and patterns were tested in a controlled fashion to elucidate possible relationships between the stimulus parameters and properties of the signal response.

Imaging

The modified fundus camera was positioned to optimize focus and even illumination of the fundus image. The imaging plane was typically at, or slightly deeper than, best focus for the retinal vessel arcades, positioned between 0° and 30° from the area centralis. The retina was illuminated with NIR light from a tungsten incandescent bulb (Fig. 1). The interrogation light was filtered with narrow or wide band-pass

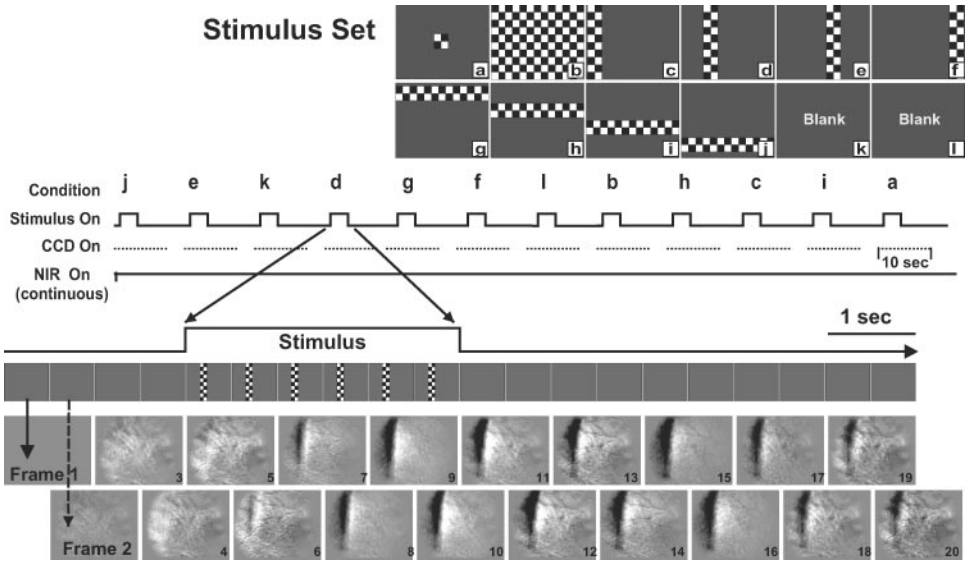

FIGURE 2. Stimulus set and imaging paradigm. *Top*: a sample stimulus set. The checkerboard patterns were typically counterflickering at 5 Hz in a 50% duty cycle. In addition to this set, an identical set of static, solid bar stimuli were used. The stimulated field was matched with the imaged field of view (i.e., condition b stimulated 26° height by 35° across). Stimuli were filtered with a 540 ± 30 nm band-pass filter, unless otherwise noted. Stimulus conditions were presented in a random sequence. *Middle*: stimulus presentation sequence and functional image development progression. *Bottom*: a representation of the stimulus presentation sequence with each frame showing 500 ms stimulus time interval. Most of the data presented in this article were generated from the following sequence: 2 seconds, stimulus off; 3 seconds, stimulus on; 5 seconds, stimulus off. Below the stimulus presentation frames is an image-development sequence. Each frame was generated by $Fr_n - Fr_0$. Baseline signal (0–2 seconds) shows minimal optical change from Fr_0. The signal developed and grew in intensity from 2 to 5 seconds (stimulus ON time). The recovery phase shows a slow decay of the signal back toward the baseline reflectance after the stimulus was turned off (5–10 seconds).

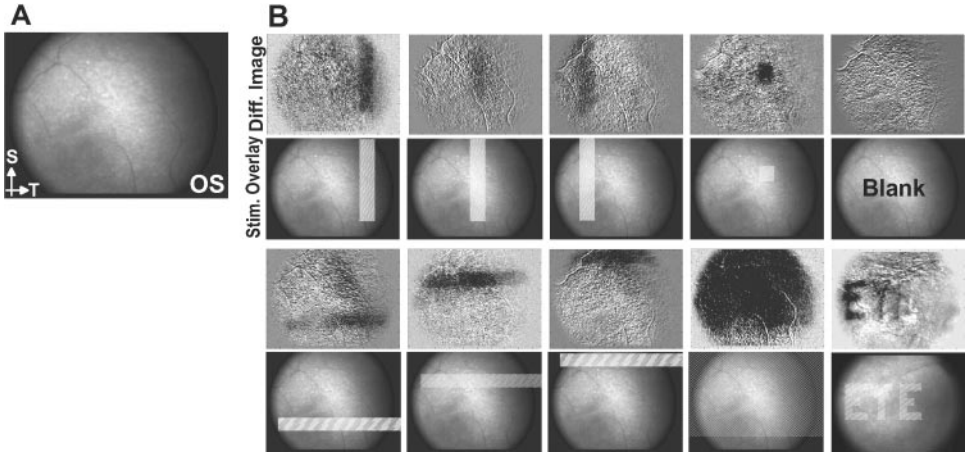

FIGURE 3. NIR reflectance images of the retina in response to patterned visual stimuli. (**A**) Baseline fundus reflectance image of the left eye at 750 ± 10 nm. Focus was maximized for clarity of the surface retinal vasculature. Superior (S) and temporal (T) directions are shown in the *bottom left corner*. Field of view spans approximately 35° in the nasal–temporal axis. (**B**) Difference images (*top*), show the change in NIR reflectance in response to visual stimulation at 540 nm. For reference, the stimulus positions are overlaid on the baseline fundus image below. The reflectance changes of the retina show tight spatial correlation with the spatial pattern used to stimulate the retina. *Dark regions*: relative decrease in NIR reflectance. Difference images were cropped 3% on the top and bottom for display purposes.

filters ranging from 700 to 900 nm (Edmund Optics, Inc. and Ealing Optics, Inc., Rocklin, CA). The power output of the NIR light was no greater than 1.6 mW, and typical values were in the range of 10 to 1000 μW. The reflectance response of the retina was filtered through a dichroic mirror (with long-pass transmission above 700 nm) and NIR-pass filter (RT-830; Edmund Optics) in series before acquisition by a CCD camera (Photometrics, Ltd.). Images were typically acquired at a rate of 2 Hz in a 192 × 144-pixel array (384 × 288-pixel resolution, binned 2 × 2 to improve the signal-to-noise ratio). Image acquisition was synchronized to the ECG and the respiration cycle to allow subtraction of respiration noise. A typical imaging trial consisted of collecting 2 seconds of baseline activity, 3 seconds of stimulus-driven activity, and 5 seconds of signal recovery (Fig. 2). Signal development was viewed in real time via a color display and data were stored for further analysis.

Image Analysis

Stored digital image files were loaded into commercial software (MatLab; The Mathworks, Inc., Natick, MA) and processed by a custom program. Sequential difference images were generated by subtracting one or more reference frames collected during baseline activity from the subsequent imaged frames in an imaging series (Fig. 2).

$$\mathrm{Diff}_{(n)} = \mathrm{Fr}_n - \mathrm{Fr}_0 \quad (1)$$

where Fr is the frame, n is the frame number in an imaged sequence, and Fr_0 is the reference image (baseline), typically the first and second frame average of the imaging sequence where no stimulus is presented.

A specific region of interest (ROI) in the image was selected to examine the magnitude and time course of the functional signal development. Fractional reflectance time course, $dR/R_{(n)}$ was calculated for a selected ROI as a function of time through the imaged sequence:

$$\mathrm{ROI}\ dR/R_{(n)} = \frac{(\mathrm{ROI}_n - \mathrm{ROI}_0)}{\mathrm{ROI}_0} \quad (2)$$

where R is 12-bit reflection intensity value, dR is the change in value from the reference frame. ROI is a user-defined x-by-y region of interest in the image held constant for each $\mathrm{Fr}_{(n)}$. ROI_0 measures the baseline reflectance for the specified region of interest. Typical ROIs used in the analysis here were 11 × 11-pixel regions (~1.5°–1.9° field of view). The ROIs were manually positioned over regions with strong reflectance patterns (see Fig. 4).

RESULTS

Spatial Properties of Stimulus-Evoked Signals

When the retina was stimulated with patterned visual stimuli, we observed focal activations colocalized with the stimulated region of retina. The appropriate filters in the path of the camera have removed visible wavelengths and thus the patterns displayed here demonstrate a stimulus-evoked change in NIR reflectance, not stimulus energy. Figure 2 shows the development sequence of the functional signal response to a vertical bar stimulus. Two predominant signals were observed within 500 ms of stimulus onset: a negative signal (dark regions) corresponding to a relative decrease in reflectance and an adjacent positive signal (pale regions) corresponding to a relative increase in reflectance compared with baseline (Fr_0). The signals often showed a spatial asymmetry: The negative signal was coextensive with the stimulated region and was unilaterally flanked by a signal of positive polarity (stimulus locations were calibrated with the camera's field of view). Of note, the positive signal was not found surrounding the entire negative signal. Instead, it showed a superior–nasal bias to the negative signal (see Figs. 2, 4). The negative signal was observed in each of the seven cats, whereas the positive signal was inexplicably absent in a small fraction of experiments. We have not been able to establish what conditions give rise to the presence or absence of the positive signals (see the Discussion section). Figure 3 shows an example of the tight spatial correlation of the negative signal response to several horizontal and vertical bars, while the positive signal is absent.

The point spread function for both positive and negative signals produced steep slopes at signal borders. We observed signals ≥ 2 SD above baseline values within 22 minutes of arc. In the cat eye,[16] this corresponds to a spatial resolution of 79.1 μm, which is on par with the resolution reported in early neocortical intrinsic signal imaging.[3,17] A demonstration of the

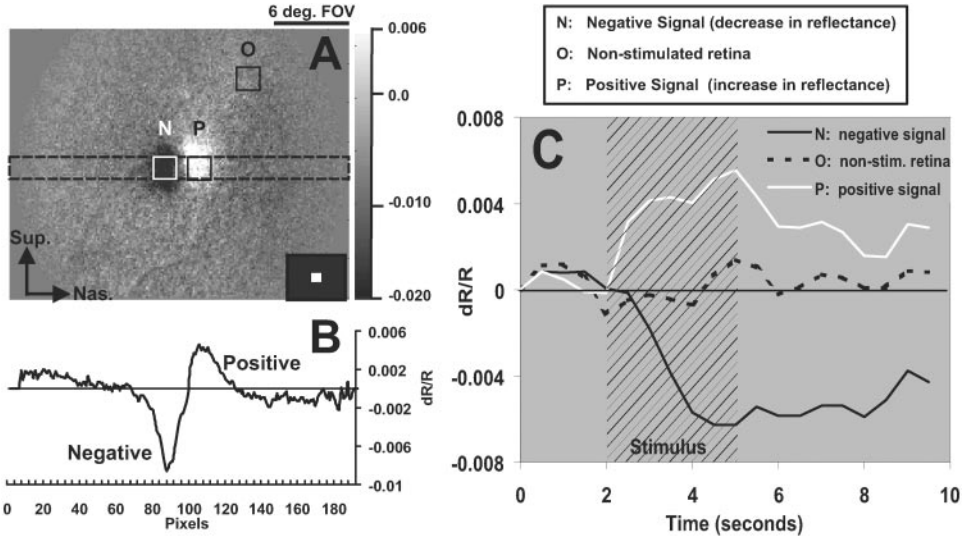

FIGURE 4. Signal spatial properties and time course. (**A**) Signal response to a 7.7-cd/m^2 spot stimulus on a 0.12-cd/m^2 background. The NIR reflectance changes produced two predominant signals: a negative signal (N) and a positive signal (P) that were spatially adjacent. The response was localized with the stimulated retina. Scale bar, 6° of the visual angle. *Arrows*: superior and nasal directions in the fundus image. *Inset*: the stimulus used to evoke the response. (**B**) A horizontal line profile of the signal. The average intensity values of rectangular region in (**A**) are plotted as a function of pixel values from the functional image above. The negative signal shows a clear dip below baseline reflectance and, nasally adjacent, a positive signal of lesser magnitude. (**C**) Fractional reflectance time course of three ROIs. Both the positive (ROI P, *white*) and negative (ROI N, *black*) signals showed minimal deviation from baseline during the first 2 seconds (stimulus off). From 2 to 5 seconds (stimulus on) both signals developed and grew in magnitude. Between 5 and 10 seconds (stimulus off), the signals had a slow recovery phase back to baseline reflectance. A third ROI (O, *dashed lines*) is also plotted. There was minimal change in reflectance for this ROI, demonstrating the signals were tightly coupled to the stimulated retina.

high resolution of the technique can be seen in Figure 3 where letters can be spelled out on the retina.

In addition, a line profile of the reflectance signal shows several interesting features including the sharpness of the signal borders and a nasal bias of the positive signal relative to the negative signal (Fig. 4). Analysis of the difference images revealed that the signals are focal, not diffuse responses across unstimulated regions of the retina. A nonstimulated region of retina (ROI O) showed a negligible change in reflectance of ± 0.0015 *dR/R* (Fig. 4C), a value less than 1 SD from the mean blank noise levels.

The field of view of the fundus camera was 27° to 35°. In separate experiments, we were able to observe signals across a much wider expanse of the retina by adjusting the azimuth and angle of the fundus camera to construct a montage. Although signals were observed across the entire retina (data not shown), we focus on the signals located approximately 0° to 35° from the area centralis. We were unable to find any evidence of a spatial relationship between the signals and the inner retinal vasculature (Fig. 3). Both negative and positive signals remained consistent across vessel boundaries.

Signal Magnitude and Time Course

Both the negative and positive signals showed a slow rise time of seconds, similar to the signals observed in the cortex.[2] We quantified the intensity of the signal by calculating the fractional reflectance change in ROIs (equation 2). The results from a typical signal time course can be seen in Figure 4 where three example ROIs are plotted to illustrate the temporal properties of the signals. The ROIs positioned over the positive (P), and negative (N) regions showed negligible changes in reflectance during the first 2 seconds of recording in which no stimulus was presented. Both the positive and negative signals arose within 500 ms of stimulus onset (Fig. 4C). The intensity of both signals monophasically increased with opposing polarity during the stimulus presentation epoch (3 seconds). On termination of the stimulus, both signals slowly decayed back toward baseline. A third ROI representing a nonstimulated part of the retina (O) is also plotted. Little change in optical reflectance was observed in this region. This result further demonstrates that the signal is spatially specific to the stimulated region of retina. In addition, the reflectance time course at ROI O shows that the signals do not propagate laterally in a wave of activity.

The slow rise and recovery time of these signals demonstrate that the signals were not an artifact of the stimulus light (540 ± 30 nm FWHH). The stimulus was presented in a step-wise epoch, whereas the positive signals recorded showed a progressive rise time and remained long after the stimulus is terminated (Figs. 2, 4). Also of interest, small fluctuations in the relatively smooth and slow signal time course seen in Figure 4 are characteristic of the noise inherent in the biological system. Fast-Fourier transform analysis (FFT) showed that the in vivo noise is strongly linked to the cyclic heart rate and respiration artifacts (FFT data not shown). We have devised image-processing filters to remove the heart rate and respiration cycle components from the intrinsic signals; however, the data presented are unfiltered, demonstrating the strength and reliability of the signal, even in the presence of noise. Exceptional imaging conditions (using 3–8-cd/m^2 stimuli and the paradigm depicted in Fig. 2) produced negative reflectance values in excess of 5% change in reflectance, whereas the positive signal magnitude was often less (Fig. 4). Some analyses were limited to the negative signal, because of the elusiveness of the positive signal.

Signal Growth Function Showing a Monophasic Time Course

In one experiment, we extended the stimulation and acquisition time to better understand the temporal dynamics of the signal. In this paradigm, we kept the stimulus onset constant and increased the stimulus duration from 0.5 to 30 seconds. Interstimulus time intervals were also increased to 30 to 60 seconds to allow for adequate recovery time. The negative signal response to different stimulus durations can be seen in Figure 5A. Longer stimulation durations generated greater signal magnitudes. The signals grew in strength in a monophasic fashion for the duration of the stimulus presentation—notably different from the signals observed at wavelengths near 600 nm in the cortex that show a biphasic[2] or triphasic time course.[18] In addition, the large overlap of the leading edge of each duration record showed the consistency of the imaging technique (Fig. 5A).

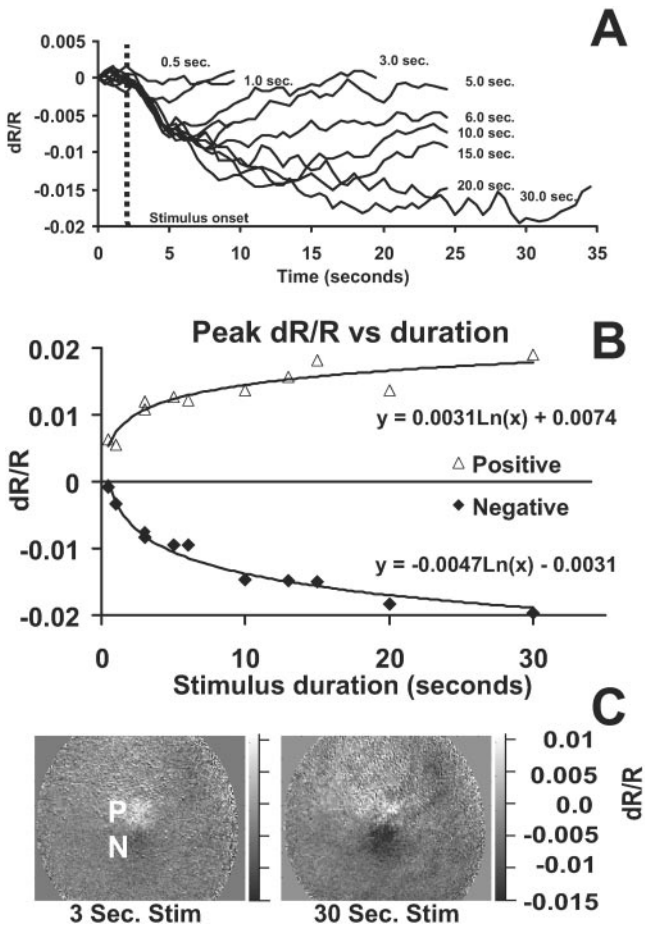

FIGURE 5. Effect of stimulus duration on signal properties. (**A**) Fractional reflectance time course for nine different stimulus durations. Several ROIs centered over negative signal hot spots for different stimulus locations (not shown) were used for this analysis. The fractional change in reflectance grew in magnitude as a function of time. Stimulus onset times were identical in each duration condition. Short stimulus durations produced low signal magnitude whereas sustained durations produced substantially greater signal. The leading edge of each data plot shows large overlap, demonstrating the consistency in the imaging technique. A similar plot with opposite polarity was obtained for the positive signal, not shown here to reduce clutter. (**B**) Signal magnitude as a function of stimulus duration. Both the positive and negative signal greatest magnitudes were plotted as a function of stimulus duration. The response for both signals initially shows strong growth. Signals continue to grow with longer durations but the rate of growth decreases. The data were fitted with a logarithmic function and show similar fit. (**C**) Functional images of a stimulus response to short and long stimuli. Both images are plotted on the same intensity scale and thus qualitatively show the difference in signal magnitude. The figures show the spread of the signal remains consistent over the time points examined, only signal intensity varies. In addition, the spatial offset of the negative and positive signal remain consistent over this time period.

The positive signal showed a similar growth trend, but with opposite polarity. Both signal magnitudes were plotted as a function of stimulus duration (Fig, 5B). Initially, the signal magnitude showed rapid growth at small increments in duration; the signal growth then plateaued. The data are fitted well by a logarithmic function. Of particular interest is the similarity of the growth functions for the positive and negative signals. This similarity may indicate that each signal has a similar biophysical origin. The signals remained localized with longer stimulus durations (Fig. 5C). Signal strength continued to grow, yet there was minimal lateral spread when stimulus durations changed by a full order of magnitude. Furthermore, the asymmetric organization of the negative and positive signal remained constant at all durations tested.

Dependency of Negative Signal on Temporal and Spatial Contrast

To investigate the signal's dependency on temporal and spatial contrast, we compared the responses to static and counterflickering stimulus conditions. A uniform green bar (7.7 cd/m^2) presented on a dark background (0.12 cd/m^2) for 3 seconds yielded a stronger response than a counterflickering bar presented for the same time (Fig. 6). The time-averaged energy of the counterflickering bar was half the luminance of the static bar due to the 50% duty cycle of the flickering stimulus. We then decreased the luminance of the static bar to exactly half of the original value so that the bar appeared as a uniform "dim green". In this condition, the counterflickering and static conditions were equivalent in time-averaged energy. A comparison of the signals under matched energy conditions revealed that the magnitude and time course were nearly identical (Fig. 6). These results demonstrate that the reflectance signal is dependent on the intensity of the stimulus, not the flickering spatiotemporal dynamics. Moreover, these results suggest that modulated ganglion cell activity (which is maximally stimulated with spatiotemporal contrast) did not drive the predominant optical signals that we observed. An accompanying paper in this journal demonstrates that the intrinsic signals show little or no spatial frequency tuning.[15]

Wavelength-Dependent Signal Spectra

To better understand the possible biophysical origins of the signal, we examined the signal dependency on illumination wavelength. In these experiments performed on six cats, we randomized the use of six narrowband filters (band-pass of 10 nm at FWHH) to test the spectral response. We plotted the magnitude of the signal as a function of wavelength to reveal the signal spectral dependence (Fig. 7A). The nega-

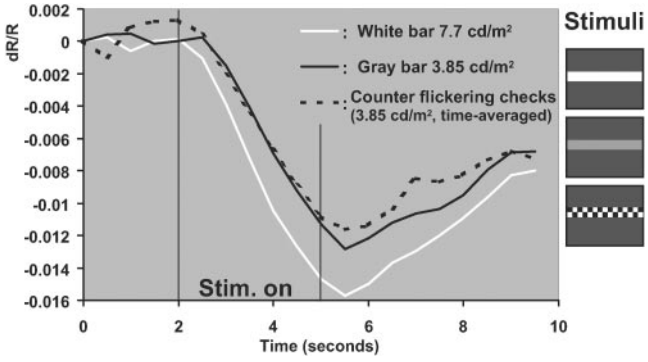

FIGURE 6. Signal dependence on counterflickering stimulus. (**A**) Fractional reflectance time course for the negative signal in response to static and dynamic stimuli. A static "green" bar (7.7 cd/m^2, example stimulus at *right*) was presented for 3 seconds and generated a strong response magnitude (*white line*). This response was consistently greater than a counterflickering stimulus (*dashed lines*; check size = 1.6 deg. FOV, 10 cyc/s; Michelson contrast, 96.8%). The time-averaged energy of the static bar was set equal to the time-averaged energy of the counterflickering stimulus (3.85 cd/m^2). This stimulus appeared as a solid "dim green" (*middle right*) and is shown by the *solid black line* in the figure. The signal magnitude and time course of the matched-energy solid stimulus and counterflickering condition were nearly identical. The stimulus was maximally driven by relative stimulus energy and minimally driven by the dynamic components of the stimulus.

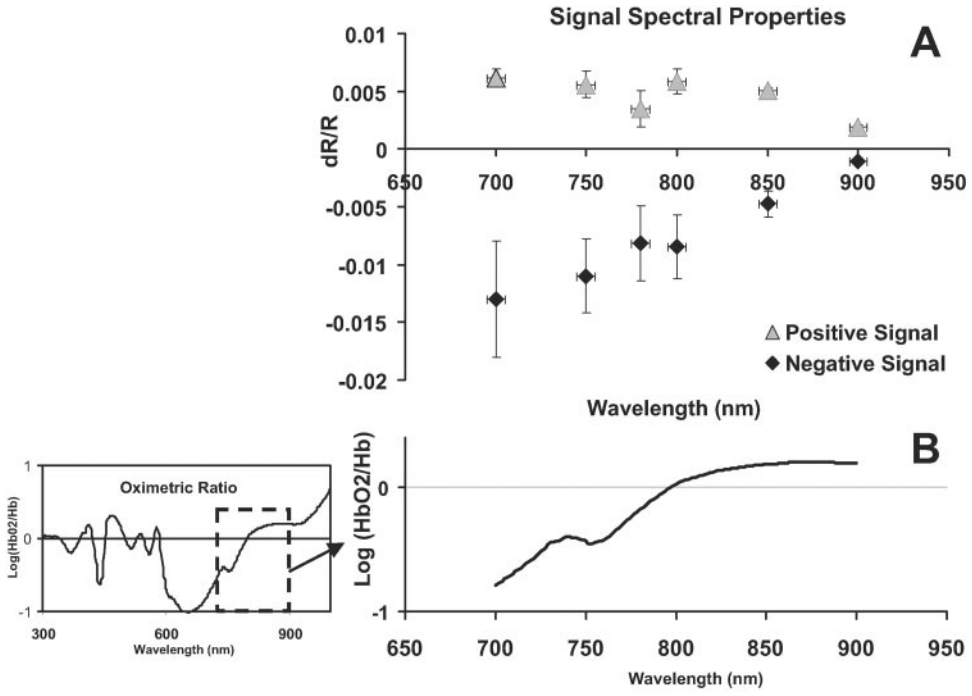

FIGURE 7. Signal dependence on interrogation wavelength. (**A**) Six narrow-band illumination filters (10 nm FWHH) were randomly presented to test the signal intensity as a function of illumination wavelength. Both the negative and positive show decreasing signal magnitude with increasing illumination wavelengths. The negative signal magnitude is greater than the positive signal, especially at shorter wavelengths. Negative data are averaged from seven experiments conducted on six cats. Both signals show a dip in spectral magnitude at ~780 nm. It is possible that the symmetry of these two signal spectra may indicate a similar biophysical origin. Positive data are averaged from four experiments on three cats. Vertical error bar, ±1 SEM. Horizontal error bars, limits of each band-pass filter at FWHH. (**B**) *Left*: the log relative oxy-/deoxyhemoglobin (HbO_2/Hb) absorption ratio, plotted as a function of wavelength. *Right*: the region corresponding to the NIR wavelengths, magnified and aligned to the intrinsic signal data. The oximetric ratio shows a decreasing absorption difference between the two hemoglobin states with longer wavelengths. This trend is similar to the intrinsic signal magnitudes we observed in (**A**). However, the negative and positive signals do not flip polarities at 800 nm, indicating that the signal cannot be purely of oximetric origin.

tive signal magnitude decreased with longer wavelengths. The positive signal showed a similar scaled phenomenon with opposite polarity, and it held true not only for the averaged population response seen in Figure 7, but with every cat we tested.

The magnitudes of both signals measured between 700 to 900 nm exhibit a reduction with increasing wavelength. By way of comparison, the oximetry signal shows a similar trend over the same spectrum (Fig. 7B). However, it is unlikely that the oximetric source is the only contributing biophysical origin of these intrinsic signals since the polarity of neither the positive nor the negative signal reverses above the isobestic wavelength (approximately 800 nm) as would be expected from a signal source purely of oximetric origin (Fig. 7B). Although other possible signal mechanisms cannot be ruled out, the overall spectral dependency of the negative and positive signals are nevertheless consistent with a hemodynamic signal (see the Discussion section).

Effects of Inverted Contrast Stimuli on Signal Polarity

The signals presented thus far have demonstrated the signal properties in response to a luminous stimulus on a dark background. To examine the spatial asymmetries of the positive and negative signals, we probed the retina's response to an inverted contrast stimulus, (a dark 0.12-cd/m^2 stimulus presented on a light 7.7-cd/m^2 background; Fig. 8). The positive and negative signals evoked from the inverted contrast stimulus reverse their phase. That is, a retinal region that initially demonstrated a negative response under a stimulus increment (presentation of a light bar) became a positive response under a stimulus decrement (dark bar on a light background). Likewise, the adjacent region that demonstrated a positive response to a light bar, became a negative signal when presented with a dark bar. An interesting observation was that regardless of the signal polarity, the strongest signals were observed underlying the visually stimulated retina (Fig. 8A;

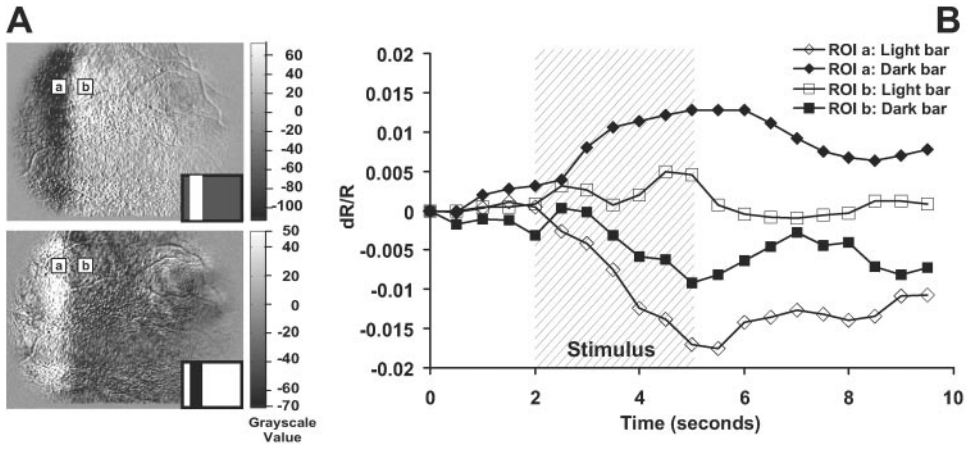

FIGURE 8. Signal polarity reversed when stimulus contrast was inverted. (**A**) *Top*: response to a luminous bar on a dark background. A strong negative signal was flanked (nasally) by a relatively weaker positive signal. *Right*: The fractional reflectance time course of ROI a and ROI b. *Bottom*: Signal response to inverted-contrast stimulus. When the stimulus background is made bright, a dark bar becomes the stimulus. The negative and positive signal polarities invert. (**B**) Fractional reflectance time course of two ROIs under normal and contrast-inverted stimulus conditions. The polarity of ROI a and ROI b inverted when stimulus contrast was reversed. ROI a, which showed a strong negative signal with the luminous bar condition yielded a strong positive signal when presented with a dark bar. Likewise, the flanking ROI b, which produced a weaker positive signal under the luminous bar condition, yielded a weak negative signal in the dark bar condition.

ROI a) and were weaker in the adjacent regions (Fig. 8A; ROI b). The magnitude of these two ROIs can be seen in Figure 8B. This result suggests the underlying signal mechanisms exhibit linearity.

Discussion

Imaging of intrinsic signals in the cortex has provided important insights into the functional architecture of the brain surface. We saw similar intrinsic signals in the cat retina. We observed two predominant signals in the NIR range: a negative and a positive signal. With a stimulus intensity increment, a negative signal is coextensive with the stimulated retina whereas a weaker positive signal lies adjacent. The evoked activity is highly localized with both positive and negative signals growing in strength over prolonged stimulus durations.

The retinal signals have a rise time on the order of seconds, temporally similar to the intrinsic signals observed in the cortex[1–4] and BOLD response in functional magnetic resonance imaging (fMRI).[19] The cortical studies have attributed the signal to a relatively slow hemodynamic response to active neural regions. In the retina, clear intrinsic signals are present within 500 ms of stimulus onset. However, unlike cortical signals measured in the 600 to 650 nm range, we did not observe a peaking response before the stimulus was turned off.[2] Instead, both signals continued to grow in intensity as long as the stimulus remained on (Fig. 5). The rate of growth for the negative and positive signals is strikingly similar, contributing evidence that both signals have a common biophysical origin.

Although there may be a dominant origin in the retina, it is likely that the signals have multiple biophysical origins with various contributions in strength, spectra, and time. Among the strongest contributors in the cortex are the spectral absorbance changes linked to hemodynamics.[2,4] There are several lines of evidence that the retinal signals may also arise from hemodynamic origins. Stimulus-evoked blood flow changes have been observed in the retina with laser Doppler flowmetry.[20–22] Similarly, it has been proposed that evoked reflectance signals are associated with local changes in hemodynamics.[8] Certainly, the existence of a BOLD response in retinal fMRI studies adds supporting evidence for the possibility of an optical hemodynamic signal.[23] As for the source of the blood volume changes, it is known that the feline retina (like many mammalian retinas) is fed by two circulation systems: the retinal circulation which branches from the optic nerve head and spreads across the superficial retina, and the choroidal circulation, a dense fenestrated bed of capillaries feeding the outermost retinal layers.[24] We did not observe any unique signal properties in relationship to the visible inner retinal circulation. Signals traversed across major retinal vessels without any notable changes in signal polarity or strength. Our technique at present does not have the depth resolution to test the relative contributions from these two circulation systems. Regardless of which vascular bed the signals may arise from, the spatial asymmetry of the signals could represent a blood-stealing effect where active neural regions divert blood resources from the surrounding microcirculation.[19] In both the left and right eyes, we observed that the positive flanking signal typically occupies the region nasal and superior to the stimulated region. This observation may correlate with flow directionality of the choroid, but further investigation is needed.

A second hemodynamic origin described in the cortex is the oximetric signal.[2,25,26] This optical change is based on the ratio of the spectral absorbance properties of oxy- and deoxyhemoglobin. The spectral dependence of the retinal signals shows a decrease in signal strength with longer wavelengths. It is notable that the oximetric function at these wavelengths showed the same trend: a decrease in magnitude from 700 to 900 nm. The polarity of both positive and negative signals can be explained by the oximetric trend at these wavelengths. For example, a change from an oxy- to deoxyhemoglobin state can show opposite signal polarity when compared with a tissue that transforms from a relatively deoxy- to oxyhemoglobin state, which happens at the level of the light-stimulated photoreceptors.[27] Despite consistent trends between intrinsic signal wavelength dependency and the oximetric function, the intrinsic signals we observed cannot be purely of oximetric origin. Neither the positive nor the negative signal reverses polarity at wavelengths longer than the isobestic one (800 nm), which implies that the signal, if hemodynamic, must have an appreciable blood volume component. An example of this may represent immediate change in the metabolic consumption driving an oximetry signal, in addition to a neurovascular coupling response that would induce reflectance changes of hemoglobin density. This combined response has been reported in the cortex.[25]

Although our results suggest a hemodynamic origin of these signals, we must consider contributions from other biophysical mechanisms, such as the expected light-scattering signals also seen in cortex[2] and in the in vitro retinal studies of Yao and George.[7] Indeed, there are certain additional aspects of our results that we have yet to reconcile with a dominant hemodynamic signal mechanism. Perhaps foremost is the expectation that the signals should reflect a *decrease* in metabolic demand with light stimuli, at least to the extent to which these signals are due to photoreceptor activity.[15] Similarly, it has been shown that oxygen utilization decreases and oxygen tension increases in the outer retina with light stimulation.[27] These facts do not seem to be compatible with the notion of an increase in blood volume with light stimulation. Further studies are needed to distinguish among the contributions of the various possible biophysical signal sources.

Regardless of the specific origin, it should be emphasized that the slow rise and decay of the positive signal indicates that the signal is not an artifact of stimulus energy (Figs. 2, 4). If stimulus energy leaked through imperfect filters, an artifact would be marked by a stepwise onset and offset marking the stimulus epoch; however, this was clearly not the case. Moreover, a negative signal (decrease in reflectance) cannot be an artifact from an increment in stimulus intensity.

The plateaued response in the retina is noticeably different from the biphasic or triphasic[18] response in the cortex. These temporal characteristics may reflect a biophysical, metabolic or possibly a tissue-specific spectral difference in the two systems. In the cortex, the dominant signals between 500 to 700 nm are predominantly from a blood volume component, whereas NIR signals have been ascribed to light-scattering effects.[17] The monophasic characteristic of the retinal signals were more analogous to cortical signals measured in the NIR wavelengths[2,25] than cortical signals measured in the 500 to 700 nm range.

Several papers have reported the presence of "fast" intrinsic optical signals on the order of milliseconds that correlate with the electrical components of the ERG[7] or optical changes attributed to light-scattering properties of active photoreceptors.[6,28–30] The light-scattering properties of stimulated neurons have been described in detail,[5] and we consider these changes as plausible origins of the intrinsic signals we report in this study. It is important to note, however, that hemodynamic and oximetric signals were notably absent from the above in vitro studies. Therefore, it is difficult to make direct comparisons with their findings and ours performed in a naturally perfused living model. Furthermore, the signals recorded from our paradigm were much slower, on the order of seconds as opposed to the milliseconds of those observed by Yao and George.[7] Yet, regardless of the preparation and temporal discrepancy, there appear to be qualitative similarities to the in

vitro fast signals, especially the spatial properties of two polarities occupying adjacent regions.

In regard to the anatomic origins of the intrinsic signals, the evidence thus far suggests a minimal ganglion cell–driven component. Our accompanying paper shows that there was little or no signal tuning when different spatial frequencies were probed.[15] We find that the signal is driven primarily by stimulus intensity and duration (Figs. 5, 6), properties much more akin to photoreceptors than ganglion cells. Moreover, if the signals are indeed metabolic in nature, photoreceptors would be a leading candidate for a dominant metabolic drive.

Further investigations may demonstrate that this study and the accompanying paper[15] provide data consistent with previous literature, that the major metabolic consumption in the retina originates from the energy needed to maintain the dark current in photoreceptors.[27,31–34]

The scope of this project has been to elucidate the general properties of the intrinsic signals in the normal condition. In this study, we have demonstrated the high spatial resolution capabilities of this technique and propose that intrinsic signal optical imaging of the retina may be a suitable tool for filling an important gap between the single-cell response and the systemic interactions of the retina in vivo. A next step in this research is to examine the signal properties in pathologic retinas. We speculate that this technique may be useful for assessing degenerative diseases.

Acknowledgments

The authors thank Mark Zarella, Dorothy Joiner, and Sandra McGillis for help with data collection and review of the manuscript.

References

1. Grinvald A, Lieke E, Frostig RD, Gilbert CD, Wiesel TN. Functional architecture of cortex revealed by optical imaging of intrinsic signals. *Nature.* 1986;324:361–364.
2. Frostig RD, Lieke EE, Ts'o DY, Grinvald A. Cortical functional architecture and local coupling between neuronal activity and the microcirculation revealed by in vivo high-resolution optical imaging of intrinsic signals. *Proc Natl Acad Sci U S A.* 1990;87:6082–6086.
3. Ts'o DY, Frostig RD, Lieke EE, Grinvald A. Functional organization of primate visual cortex revealed by high resolution optical imaging. *Science.* 1990;249:417–420.
4. Fukuda M, Rajagopalan UM, Homma R, Matsumoto M, Nishizaki M, Tanifuji M. Localization of activity-dependent changes in blood volume to submillimeter-scale functional domains in cat visual cortex. *Cerebral Cortex.* 2005;15:823–833.
5. Cohen LB. Changes in neuron structure during action potential propagation and synaptic transmission. *Physiol Rev.* 1973;53:373–418.
6. Pepperberg DR, Kahlert M, Krause A, Hofmann KP. Photic modulation of a highly sensitive, near-infrared light-scattering signal recorded from intact retinal photoreceptors. *Proc Natl Acad Sci U S A.* 1988;85:5531–5535.
7. Yao XC, George JS. Dynamic neuroimaging of retinal light responses using fast intrinsic optical signals. *Neuroimage.* 2006;33:898–906.
8. Nelson DA, Krupsky S, Pollack A, et al. Special report: noninvasive multi-parameter functional optical imaging of the eye. *Ophthalmic Surg Lasers Imag.* 2005;36:57–66.
9. Hickam JB, Frayser R, Ross JC. A study of retinal venous blood oxygen saturation in human subjects by photographic means. *Circulation.* 1963;27:375–385.
10. Barriga ES, Pattichis M, Ts'o D, et al. Spatiotemporal independent component analysis for the detection of functional responses in cat retinal images. *IEEE Trans Med Imag.* 2007;26:1035–1045.
11. Abramoff MD, Kwon YH, Ts'o D, et al. Visual stimulus-induced changes in human near-infrared fundus reflectance. *Invest Ophthalmol Vis Sci.* 2006;47:715–721.
12. Tsunoda K, Oguchi Y, Hanazono G, Tanifuji M. Mapping cone- and rod-induced retinal responsiveness in macaque retina by optical imaging. *Invest Ophthalmol Vis Sci.* 2004;45:3820–3826.
13. Hanazono G, Tsunoda K, Shinoda K, Tsubota K, Miyake Y, Tanifuji M. Intrinsic signal imaging in macaque retina reveals different types of flash-induced light reflectance changes of different origins. *Invest Ophthalmol Vis Sci.* 2007;48:2903–2912.
14. Grieve K, Roorda A. Intrinsic signals from human cone photoreceptors. *Invest Ophthalmol Vis Sci.* 2008;49:713–719.
15. Schallek J, Kardon R, Kwon Y, Abramoff M, Soliz P, Ts'o D. Stimulus-evoked intrinsic optical signals in the retina: pharmacologic dissection reveals outer retinal origins. *Invest Ophthalmol Vis Sci.* 2009;50:4873–4880.
16. Vakkur GJ, Bishop PO. The schematic eye in the cat. *Vision Res.* 1963;3:357–360.
17. Lieke EE, Frostig RD, Arieli A, Ts'o DY, Hildesheim R, Grinvald A. Optical imaging of cortical activity: real-time imaging using extrinsic dye-signals and high resolution imaging based on slow intrinsic-signals. *Annu Rev Physiol.* 1989;51:543–559.
18. Chen-Bee CH, Agoncillo T, Xiong Y, Frostig RD. The triphasic intrinsic signal: implications for functional imaging. *J Neurosci.* 2007;27:4572–4586.
19. Shmuel A, Yacoub E, Pfeuffer J, et al. Sustained negative BOLD, blood flow and oxygen consumption response and its coupling to the positive response in the human brain (see comment). *Neuron.* 2002;36:1195–1210.
20. Riva CE, Logean E, Falsini B. Visually evoked hemodynamical response and assessment of neurovascular coupling in the optic nerve and retina. *Prog Retin Eye Res.* 2005;24:183–215.
21. Shakoor A, Blair NP, Mori M, Shahidi M. Chorioretinal vascular oxygen tension changes in response to light flicker. *Invest Ophthalmol Vis Sci.* 2006;47:4962–4965.
22. Riva CE, Harino S, Shonat RD, Petrig BL. Flicker evoked increase in optic nerve head blood flow in anesthetized cats. *Neurosci Lett.* 1991;128:291–296.
23. Duong TQ, Ngan SC, Ugurbil K, Kim SG. Functional magnetic resonance imaging of the retina. *Invest Ophthalmol Vis Sci.* 2002;43:1176–1181.
24. Zhang HR. SEM study of corrosion casts on retinal angioarchitecture in man and macaque monkey [in Chinese]. *Chung Hua Yen Ko Tsa Chih* [*Chin J Ophthalmol*]. 1988;24:282–285.
25. Malonek D, Grinvald A. Interactions between electrical activity and cortical microcirculation revealed by imaging spectroscopy: implications for functional brain mapping. *Science.* 1996;272:551–554.
26. Shtoyerman E, Arieli A, Slovin H, Vanzetta I, Grinvald A. Long-term optical imaging and spectroscopy reveal mechanisms underlying the intrinsic signal and stability of cortical maps in V1 of behaving monkeys. *J Neurosci.* 2000;20:8111–8121.
27. Linsenmeier RA. Effects of light and darkness on oxygen distribution and consumption in the cat retina. *J Gen Physiol.* 1986;88:521–542.
28. Lewis JW, Miller JL, Mendel-Hartvig J, Schaechter LE, Kliger DS, Dratz EA. Sensitive light scattering probe of enzymatic processes in retinal rod photoreceptor membranes. *Proc Natl Acad Sci U S A.* 1984;81:743–747.
29. Harary HH, Brown JE, Pinto LH. Rapid light-induced changes in near infrared transmission of rods in Bufo marinus. *Science.* 1978;202:1083–1085.
30. Kuhn H, Bennett N, Michel-Villaz M, Chabre M. Interactions between photoexcited rhodopsin and GTP-binding protein: kinetic and stoichiometric analyses from light-scattering changes. *Proc Natl Acad Sci U S A.* 1981;78(11):6873–6877.
31. Stefansson E. Retinal oxygen tension is higher in light than dark. *Pediatr Res.* 1988;23:5–8.
32. Alder VA, Cringle SJ, Constable IJ. The retinal oxygen profile in cats. *Invest Ophthalmol Vis Sci.* 1983;24:30–36.
33. Yu DY, Cringle SJ. Oxygen distribution and consumption within the retina in vascularised and avascular retinas and in animal models of retinal disease. *Prog Retin Eye Res.* 2001;20:175–208.
34. Stefansson E, Wolbarsht ML, Landers MB 3rd. In vivo O_2 consumption in rhesus monkeys in light and dark. *Exp Eye Res.* 1983;37:251–256.